

A model of sea-foam thickness distribution for passive microwave remote sensing applications

N. Reul and B. Chapron

Institut Français de Recherche pour l'Exploitation de la Mer, Laboratoire d'Océanographie Spatiale, Plouzané, France

Received 4 April 2003; revised 10 July 2003; accepted 30 July 2003; published 15 October 2003.

[1] Foam formations at the sea surface significantly contribute to microwave brightness temperature signatures over the ocean for moderate to high wind speeds. The thickness of foam layers generated by breaking waves follows a specific distribution due to unsteadiness of breaking and the large range of wave scales involved in the phenomenon. Although the effect of a distributed thickness-parameter on the foam-induced microwave brightness temperature may be comparable to or larger than the fractional whitecap coverage, it is not yet included in brightness models. To fill this gap, we develop a dynamical model for the conditional fraction of sea-surface covered by whitecaps with given thickness, as a function of wind speed. It is an integrated function of the foam-layer lifetime and of the distribution of the total length of breaking fronts at given scale. The depth at which air bubbles are injected into the water column is scaled with breaking front velocity using reported dynamical properties of unsteady breaking regions. For wind speed less than 20 m/s, the model predicts that two thirds of the fractional whitecap coverage is due to layers on average thinner than 60 cm and 35 cm for crest- and static-foam formations, respectively. In unstable atmospheric conditions, an increase in wind speed from 7 to 20 m/s corresponds to a coverage-weighted foam-layer thickening of about 1 cm and 3.5 cm, respectively. In neutral conditions, the thickening is approximately 2 times lower. Still, this will induce doubling of foam emissivity at Ku and C

bands. **INDEX TERMS:** 4504 Oceanography: Physical: Air/sea interactions (0312); 4275 Oceanography: General: Remote sensing and electromagnetic processes (0689); 4560 Oceanography: Physical: Surface waves and tides (1255); 0305 Atmospheric Composition and Structure: Aerosols and particles (0345, 4801);

KEYWORDS: sea foam, breaking waves, thickness, fractional coverage, microwave brightness temperature

Citation: Reul, N., and B. Chapron, A model of sea-foam thickness distribution for passive microwave remote sensing applications, *J. Geophys. Res.*, 108(C10), 3321, doi:10.1029/2003JC001887, 2003.

1. Introduction

[2] Although foam generated by breaking waves typically covers only a few percent of the sea surface, it has a profound effect on the average microwave brightness of the ocean surface [Rosenkranz and Staelin, 1972; Stogryn, 1972; Ross and Cardone, 1974; Smith, 1988; Kunkee and Gasiewski, 1997; Guo et al., 2001; Monahan, 2002; Anguelova, 2002]. For surface wind speeds greater than 15 m/s, foam-induced effects may provide as much as half of the total sea surface signature to an orbiting microwave radiometer [Droppleman, 1970; Barber and Wu, 1997].

[3] As originally proposed by Stogryn [1972], the contribution of foam formations to sea surface brightness temperature can be modeled as a function of wind speed as

$$T_{BF}(f, p, \theta, U) = F(U) \cdot T_s \cdot e_{BF}^{typ}(f, p, \theta), \quad (1)$$

where f , p , and θ are the receiving electromagnetic frequency, polarization, and incidence angle of the measuring device, respectively, $F(U)$ is the fraction of sea surface

area covered by whitecaps at wind speed U , T_s is the physical temperature of foam, usually assumed the same as the bulk sea surface temperature, and e_{BF}^{typ} is the emissivity of typical sea-foam layers.

[4] Extensive work has been conducted over the past years on the determination of $F(U)$, both experimentally [Stogryn, 1972; Ross and Cardone, 1974; Monahan and O'Muircheartaigh, 1980; Bondur and Sharkov, 1982; Monahan and Woolf, 1989; Xu et al., 2000] and theoretically [Phillips, 1985; Huang et al., 1986; Wu, 1988]. Empirical models for $F(U)$ are most often used in equation (1) to estimate the wind speed dependence of T_{BF} [e.g., Tang, 1974; Barber and Wu, 1997; Kunkee and Gasiewski, 1997]. The microwave emissivity e_{BF}^{typ} of typical sea-foam layers is usually determined using empirical formulas that are wind independent, and only functions of frequency f , incidence angle θ , and polarization p [Stogryn, 1972; Pandey and Kakar, 1982; Koepke, 1986a; Smith, 1988]. In such models for T_{BF} , the effect of changes in foam properties as a function of wind speed are therefore solely seen as changes in fractional coverage.

[5] Breaking waves at the ocean's surface inject bubbles and turbulence into the water column. During periods of

rough weather, the scales and occurrence of wave breaking will increase with increasing sea states and wind stress. An enhanced breaking activity results in deeper and more intense mixing of the surface waters and the localized turbulent transport of bubbles to depth [Terrill *et al.*, 2001]. Both whitecaps and bubble clouds are correlated via their dependence on wind speed. The air void fraction, the size distribution of bubbles within foam layers and the vertical thickness of these layers will vary greatly in space and time as a function of the synoptic wind and wave conditions.

[6] Experimental works [Williams, 1971; Norberg *et al.*, 1971; VanMelle *et al.*, 1973; Webster *et al.*, 1976; Bordonskiy *et al.*, 1978; Wilheit, 1979; Smith, 1988; Wang *et al.*, 1995; Asher *et al.*, 1998] as well as theoretical studies [Droppleman, 1970; Rosenkranz and Staelin, 1972; Dombrovskiy, 1979; Dombrovskiy and Raizer, 1992; Guo *et al.*, 2001] have shown that these structural features of foam layers are the major determinants of their microwave emissivity at given frequency, incidence angle, and polarization.

[7] In particular, variation in the vertical thickness δ of foam layers strongly alter their emissivity. For example, laboratory measurements conducted by Williams [1971] reveal that an increase of foam-layer thickness $\Delta\delta$ of about 2 mm doubles the foam emissivity at X-band [see Ulaby *et al.*, 1986, pp. 1455]. A detailed review showing the large impact of that parameter on foam-induced microwave emissivity is first given in this paper. Large effects induced by thickness variation have also been observed or theoretically predicted at differing frequency bands, with magnitude depending on the ratio $\Delta\delta/\lambda_o$, where λ_o is the electromagnetic wavelength. An important consequence is that small variations of foam-layer thickness with varying wind stress may on average have the same or even larger impact on T_{Bf} than do changes in fractional whitecap coverage. While the associated variation in the air void fraction and bubble size with foam depth may also strongly affect foam emissivity, we solely focus in the present paper on the impact of distributed foam-layer thicknesses at the sea surface. Indeed, bubble void fractions and size distributions beneath breaking waves were shown to depend on the scale (wavelength or speed) of the waves carrying the breakers [Vagle and Farmer, 1992; Lamarre and Melville, 1992]. Impact of these parameters will therefore be evaluated once a realistic distribution of foam-layer thicknesses is provided as a function of wind speed and breaking wave scale.

[8] The impact of F on the brightness temperature has received much more attention in the past than the effects of naturally distributed foam-layer thicknesses at the ocean surface and their dependence with wind speed. For example, Wilheit [1979] assumed a wind dependence for e_{Bf}^{pp} but arbitrarily fixed an overall averaged sea foam-layer thickness of 1 cm to achieve best correspondence between his theoretical calculations of T_{Bf} and experimental data. The issue of consistency of the choice for this particular value with pertinent hydrodynamic data was not addressed. Therefore, whether one uses wind-dependent forms for e_{Bf}^{pp} [Wilheit, 1979] or wind-independent formulas [e.g., Stogryn, 1972; Pandey and Kakar, 1982; Smith, 1988], the effects of change in the foam-layer thickness distribution

as a function of wind speed is not taken into account in the modeling of T_{Bf} . As a result, it remains generally unclear whether the differences between theoretical calculations and experimental data should be attributed to deficiencies of the scattering model for e_{Bf}^{pp} or to an inaccurate description of the statistical properties of sea-foam formations.

[9] When using current emissivity models for e_{Bf}^{pp} [e.g., Dombrovskiy and Raizer, 1992; Guo *et al.*, 2001] to evaluate the global impact of distributed foam-layer thicknesses on T_{Bf} , an estimate of the conditional fraction of sea surface covered by whitecaps with average thickness $\bar{\delta}$ at given wind speed U , namely $F(U, \bar{\delta})$, is thus needed. In this framework, equation (1) is then rewritten in the more general form

$$T_{Bf}(\theta, p, f, U) = \int F(U, \bar{\delta}) \cdot T_s \cdot e_{Bf}^{pp}(\theta, p, f, \bar{\delta}) d\bar{\delta}, \quad (2)$$

where $e_{Bf}^{pp}(\theta, p, f, \bar{\delta})$ is the multi-parameter dependence of foam emissivity, including foam-layer thickness impact, that can be derived from recently developed radiative transfer models.

[10] The primary objective of this paper is therefore to lay down a consistent analysis to relate fractional sea surface area covered by whitecaps to their average thickness $\bar{\delta}$. To this end, a time-dependent foam-layer thickness model for individual breakers $\bar{\delta}(t, \lambda)$, where λ is the wavelength of the underlying carrier wave, is first derived in the second section of the paper. Using self-similarity assumptions concerning the instantaneous geometry of breaking regions, the model for $\bar{\delta}(t, \lambda)$ is based on the reported dynamics of single whitecaps area [Kennedy and Snyder, 1983; Koepke, 1986b; Sharkov, 1995] and on the measured dynamical scaling of bubble clouds extent underneath unsteady breakers [Rapp and Melville, 1990].

[11] Developments and concepts originally introduced by Phillips [1985] are then used to provide the model for $F(U, \bar{\delta})$. Namely, we use his proposed definition for the whitecap fractional coverage F generated by breaking wave crests,

$$F(U) = \int_0^\infty \int_{-\pi/2}^{\pi/2} c\tau \wedge(\vec{c}, U) d\vec{c}, \quad (3)$$

where \vec{c} is the velocity of advance of underlying waves carrying a whitecap, the distribution function $\wedge(\vec{c}, U) d\vec{c}$ represents the average length per unit surface area of breaking fronts that have velocities in the range \vec{c} to $\vec{c} + d\vec{c}$ at wind speed U , and τ is the persistence time of foam layers at the surface.

[12] Various models have been proposed for the function $\wedge(\vec{c}, U)$. This function directly enters the characterization of the expected energy losses at a given surface scale. Consequently, the distribution $\wedge(\vec{c}, U)$ may be expressed through a wave spectrum definition. In a sea state at statistical equilibrium, a model for $\wedge(\vec{c}, U)$ can thus be derived using the established proportionality between dissipation and wind input sources in the wave field [Phillips, 1985]. Recently, Melville and Matusov [2002] were able to measure the distribution function $\wedge(\vec{c}, U) d\vec{c}$ in several wind forcing conditions. They show that when weighted

by U_{10}^{-3} , where U_{10} is the wind speed at 10-m height, the Λ measurements collapse approximately onto a single exponential curve. The use of incremental breaking probabilities may also be considered to determine $\Lambda(\bar{c}, U)$, such as the model for dominant breaking waves recently developed by *Makin and Kudryavtsev* [2002]. In a third section, we briefly compare these three available parameterizations for $\Lambda(\bar{c}, U)d\bar{c}$.

[13] Depending upon the choice for the form of the function Λ , we then assess the ability of the dynamical model of equation (3) to correctly reproduce measured whitecap coverages as a function of wind speed. Taking the empirical model of *Melville and Matusov* [2002] for $\Lambda(\bar{c}, U)$, and fixing the relative value of the foam-layer persistence time τ to the active breaking events duration, the model is shown to perform well for both the reported “dynamic foam” coverage associated with the breaking wave crests, and the “static foam” coverage associated with older foam formations that remain in the wake of a breaker.

[14] Classes of breaking fronts moving at a given speed are further associated with classes of foam layers having a given characteristic thickness scale $\bar{\delta}(c)$, using the previously developed model for $\bar{\delta}(t, \lambda)$. The incremental fraction $dF(\bar{\delta}, U)$ of sea surface covered by foam formations with average thickness between $\bar{\delta}$ and $\bar{\delta} + d\bar{\delta}$ at wind speed U is then deduced from the incremental model of whitecap coverage $dF(c, U)$. A correction is finally included in the modeling to account for the atmospheric boundary-layer stability effects. Results and their impact on passive microwave remote sensing of sea surface are discussed in a last section.

2. Impact of Sea-Foam Layer Thickness on the Microwave Emissivity

[15] Models proposed so far for calculating the emissivity e_{Bf}^{pp} of sea-foam formations at various incidence angles, microwave frequencies, and polarizations may be divided into two types: empirical formulas [*Stogryn*, 1972; *Wilheit*, 1979; *Pandey and Kakar*, 1982; *Smith*, 1988; *Barber and Wu*, 1997] and physically-based models [*Droppleman*, 1970; *Rosenkranz and Staelin*, 1972; *Dombrovskiy*, 1979; *Dombrovskiy and Raizer*, 1992; *Guo et al.*, 2001]. Empirical approaches for e_{Bf}^{pp} consist in fitting procedures using data from laboratory [*Williams*, 1971] as well as field experiments [*Stogryn*, 1972; *Wilheit*, 1979; *Pandey and Kakar*, 1982; *Smith*, 1988]. Theoretical models take into account the physical properties of foam formations at the sea surface and propose electromagnetic solutions to determine their specific emissivities. Between existing theoretical approaches, differences mainly lie in the way the inner structure of a typical foam layer is described within the model, but also in the type of electromagnetic scattering theory used to compute the effective dielectric constant of that layer. *Droppleman* [1970] thus modeled foam as a porous dielectric layer of air and water mixture and used a dielectric mixing model for heterogeneous materials. *Rosenkranz and Staelin* [1972], and later *Bordonskiy et al.* [1978], assumed that sea foam as probed by a microwave radiometer may be modeled as series of plane-parallel thin water films embedded in an air volume. They used a multi-layered approach to evaluate its reflectivity. In more recent studies by *Dombrovskiy* [1979], *Dombrovskiy and Raizer* [1992] and *Guo et al.* [2001], foam

layers are modeled as volumes of densely distributed sticky air bubbles coated with thin seawater coating. Dense media radiative transfer theory is then used to calculate the brightness temperatures of such layers at different microwave frequencies.

[16] Despite these conceptual differences, both empirical and theoretical approaches agree on the fact that at microwave frequencies, the emissivity of a sea-foam layer will mainly depend on the microstructure properties of the layer itself (bubble size distribution, air void fraction within the layer, strength of adhesive forces between bubbles, etc.) and on the foam-layer thickness, which is an important macro-scale descriptor of the air-water mixture.

[17] The effects of the thickness δ of foam layers on their microwave emissivities were first studied in the laboratory by *Williams* [1971]. He measured emissivities in a waveguide and found that at X-band ($\lambda_o = 3.2$ cm), an increase of the foam-layer thickness from 0 to about 2 mm increases the emissivity from about 0.4 to 0.8. Note that *Williams* [1971] carried out his tank studies using fresh water with soap to stabilize the bubbles produced. Care should therefore be taken when one tries to extend his results to sea water without surfactants. Radiometric measurements were also conducted later in the laboratory by *Bordonskiy et al.* [1978] at electromagnetic wavelengths $\lambda_o = 0.26, 0.86, 2.08, 8,$ and 18 cm in the presence of spontaneous decay of a thick foam layer ($\delta \sim 1-1.5$ cm) into a thin emulsive monolayer ($\delta \sim 0.1$ cm). They found a simultaneous decrease Δe_{Bf}^{pp} in the measured emissivity of 3%, 15%, 20%, 40%, and 14% at $\lambda_o = 0.26, 0.86, 2.08, 8,$ and 18 cm, respectively. They concluded that the decimeter range of wavelengths ($\lambda_o = 18$ cm) only reacts to layers thicker than about 2 cm. More recently, similar experimental measurements were performed by *Asher et al.* [1998] at 19 GHz ($\lambda_o = 1.6$ cm), incidence angle of 53° in vertical and horizontal polarization. As revealed, an increase of about 2 cm in sea-foam-layer vertical thickness would approximately double the emissivity.

[18] These experimental results are consistent with *Droppleman's* [1970] model and the radiative transfer calculations of *Guo et al.* [2001] at 20 and 19 GHz, respectively. Both models predict an increase of approximately 50% in foam emissivity if $\Delta\delta \simeq +2$ cm. *Guo et al.'s* [2001] model moreover reveals that the polarization and frequency dependencies of foam emissivity are also strongly thickness dependent. Saturation, i.e., foam radiations tending to a black body, thus occurs at thinner foam layers for 37 GHz than 19 GHz and depends on the polarization. In addition, *Zhou et al.* [2002] also observed emissivity saturation as the foam-layer thickness increases. They found that the four Stokes parameters level off to constant values once a threshold thickness value is reached.

[19] The main results from these studies are summarized in Figure 1, where the measured or predicted relative change in foam emissivity is plotted as a function of the ratio between foam-thickness variation and electromagnetic wavelength. A large dispersion is observed in the data, probably due to either different incidence angle and polarization conditions, or to differences in the inner structure (air void fraction, mean bubble diameters) of the foam layers considered. Nevertheless, two key points are illustrated: (1) for small variations in sea-foam thickness less than about $2\lambda_o$, changes in emissivity always larger than

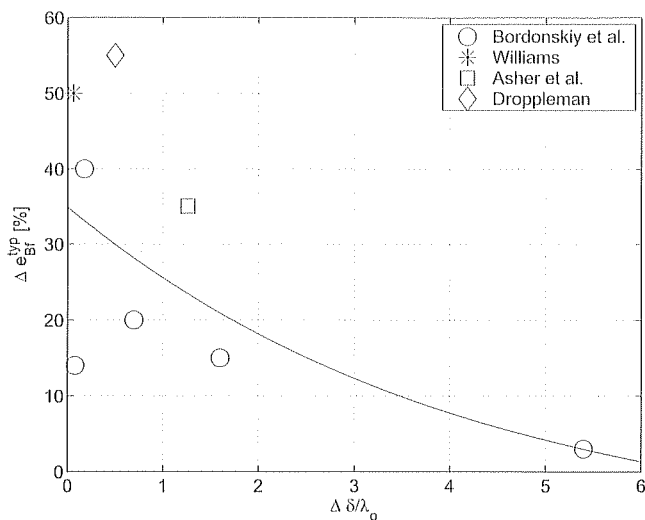


Figure 1. Relative variation Δe_{BF}^{wp} of foam emissivity as a function of variation in the thickness of foam layer $\Delta\delta$ with respect to electromagnetic wavelength λ_o ($\lambda_o = 0.26, 0.86, 2.08, 8,$ and 18 cm for *Bordonskiy et al.* [1978]; $\lambda_o = 3.2$ cm for *Williams* [1971], $\lambda_o = 1.6$ cm for *Asher et al.* [1998], and *Droppleman* [1970]).

14% are observed for a wide range of electromagnetic frequencies (they can occasionally reach 55%), and (2) for thickness variations large compare to electromagnetic wavelength ($\Delta\delta \gg 2\lambda_o$), saturation occurs and the increase in foam-induced emissivity is reduced.

[20] According to *Monahan and Woolf* [1989], fractional whitecap coverage $F(U)$ increases from about 0 to 0.12 if wind speed increases from 0 to 20 m s^{-1} . In this wind speed range, foam coverage variations therefore induce changes in foam emissivity that are always smaller than 12% (e.g., see equation 1). As already noticed by *Smith* [1988] and illustrated here, small variation in the averaged foam thickness parameter with wind stress may therefore have the same or even larger incremental effect on T_{BF} as does the fractional coverage F .

3. Dynamical Model of Whitecap Thickness for an Individual Breaker

[21] Owing to the strong unsteadiness of the breaking phenomenon and the large range of surface scales involved at sea, little is known about the dynamics of the foaming process and, consequently, about the associated vertical thickness of whitecaps. However, the dynamics of such a process have been carefully studied both in the laboratory and theoretically for the so-called quasi-steady breakers (waves produced by ships or hydrofoils moving at constant speed). For unsteady breaking waves of open seas, dynamics of associated foam layers have been mainly characterized by the evolution of the foaming patch at the surface and the mixing depth of the turbulent diphasic flows generated underneath the interface.

3.1. Quasi-Steady Breaking

[22] *Longuet-Higgins and Turner* [1974] conducted a theoretical analysis of the turbulent breaking region grow-

ing on the forward face of an individual spilling breaker. By using approximate equations of motion, combined with some related experimental data on air entrainment in free-surface flow, they were able to predict the acceleration of the front of the breaker and some aspects of the shape of the breaking region, both as a function of the wave's phase speed c and the slope θ of the forward face. Under the assumptions that the flow is steady in time and that the forward slope of the carrying wave remains constant, these authors show that the thickness of the whitecap δ is proportional to the distance measured from the crest of the wave.

[23] Since the laboratory measurements of [*Duncan*, 1981] on quasi-steady breaking waves (generated by a hydrofoil towed at a constant speed), it is further widely recognized that the overall geometry of quasi-steady spilling breaking waves may be assumed to be statistically self-similar. On average, the larger breakers are magnified copies of the smaller ones. The breaking region itself is a fixed fraction A of the cross-sectional area of the wave and is also statistically self-similar.

[24] The geometry for the whitecap as given by *Duncan* [1981] is described in Figure 2. It is very similar to the representation of whitecaps as "prism located on wave slope," as depicted by [*Bortkovskii*, 1987]. *Duncan* [1981] derived scaling laws for the following parameters describing a quasi-steady spilling breaker: the average length L_b , the average thickness $\bar{\delta}$, the area $A \simeq L_b \bar{\delta}$ of the breaking region in the main direction of propagation of the carrying wave, and the length of the breaking wave λ . He found that for quasi-steady breakers, (1) all the waves have breaking regions with the same aspect ratio $A/L_b^2 \simeq 0.1$; that is, the breaking region average vertical thickness divided by its length is a constant; and (2) the ratio between the length of the breaking region and the length of the breaking wave is the same for all conditions, $L_b/\lambda \simeq 30\%$. Accordingly, the following similarity law for the average whitecap thickness will apply:

$$\bar{\delta}(\lambda) \approx b \cdot \lambda, \quad (4)$$

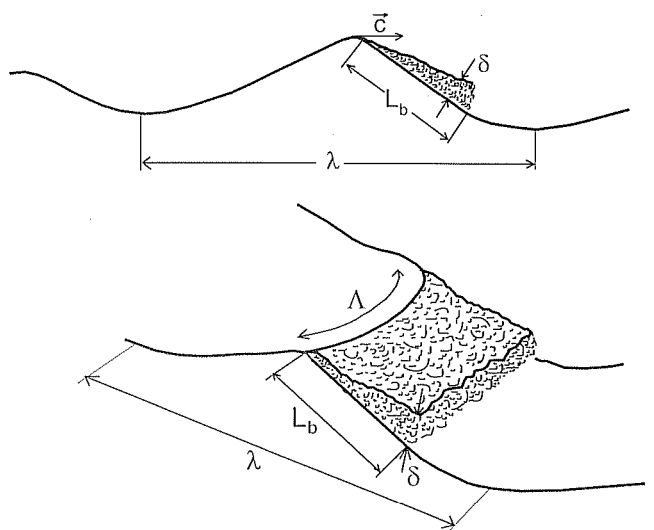


Figure 2. Sketch showing the features of a quasi-steady spilling breaker. The wave is moving from left to right and has a whitecap on its forward face.

where b is an empirical constant estimated by *Duncan* [1981] to be $b \simeq 0.03$ for quasi-steady breaking waves.

3.2. Transient Breaking Events

[25] For transient breaking events, the similarity law (equation (4)) is expected to be violated. Since the foam-layer dynamics is basically unsteady, one has in general $\bar{\delta}(\lambda, t) \neq \bar{\delta}(\lambda)$. Bubbles and turbulence are injected into the water column down to a depth which evolves significantly during a complete unsteady event since the process is driven by a transient source of motion at the surface.

[26] The growth and decay rate of unsteady whitecaps were studied by several authors in terms of the temporal evolution of the area covered at the surface by individual whitecaps [*Monahan*, 1971; *Kennedy and Snyder*, 1983; *Koepke*, 1984; *Monahan and Woolf*, 1989; *Walker*, 1994; *Sharkov*, 1995]. In these studies, reported temporal variation in whitecaps area is observed to peak rapidly during active breaking with a slower exponential decay after formation. *Monahan* [1988] suggested the terms “Stage A” and “Stage B” to classify these visual signatures of breakers. Stage A features are due to actively breaking waves, while stage B features consist of the “fossil foam” or “foam rafts” that remained in the wake of a stage A breaker. Works by *Kennedy and Snyder* [1983] and *Koepke* [1984] give support to a monotonic increase of the whitecap size during stage A. The exponential character of foam field decay (stage B) was clearly measured by *Sharkov* [1995] from analysis of time patterns of individual foam spot dissipation.

[27] Subsurface characterization of the foam layers was given by *Rapp and Melville* [1990], who measured the time evolution of the depth down to which turbulent patches generated under unsteady breaking waves do mix. Their subsurface measurements show that the turbulent region generated beneath the interface by a breaking wave with carrier wavenumber k mixes down to a depth D , with $kD \approx 0.5-1$ after four wave periods. They found that the initial deepening of the layer is very rapid during the first period after breaking, such that $kD \approx 0.3, 0.5$ within half a wave period for spilling and plunging waves, respectively. They further show that this layer is subsequently reaching an asymptotic dependence $D \propto t^{1/4}$, after one to two wave periods.

[28] Assuming that the breaking region geometry in unsteady breaking waves is also self-similar, we postulate that the respective dynamics of the foam-layer thickness and surface area are similar, so that $\bar{\delta}(\lambda, t)$ can be approximated by the following process:

$$\begin{aligned} \bar{\delta}(\lambda, t) &= \beta(\lambda)t && \text{for } 0 \leq t \leq \tau_* \\ \bar{\delta}(\lambda, t) &= \bar{\delta}_{max}(\lambda) \exp\left(-\frac{t - \tau_*}{\tau'}\right) && \text{for } t \geq \tau_*, \end{aligned} \quad (5)$$

where $\beta(\lambda)$ is the temporal rate of increase of the air-water mixture thickness during stage A, τ_* the mean duration of the active breaking event, τ' is an appropriate exponential time constant and $\bar{\delta}_{max}(\lambda)$ is the maximum thickness a foam layer generated by a breaking wave with length λ may reach.

[29] Mean duration of active breaking events τ_* was inferred from high-frequency radar measurements by

Phillips et al. [2001, Figure 4]. They found a fairly clear linear proportionality between the mean duration of the breaking event τ_* and the event speed, consistent with the relation $\tau_* = 5 (c/g) \simeq 0.8 T_b$ where T_b is the breaking wave period. As noticed by *Phillips et al.* [2001], *Rapp and Melville* [1990] also found that this expression summarized well their laboratory measurements. If we further define the “wavelength” of the breaker as $\lambda = 2\pi c^2/g$ using the dispersion relationship for gravity waves in deep water, then $\tau_* \approx 0.64\lambda^{1/2}$.

[30] To determine the temporal rate β of increase of an individual foam-layer thickness during stage A, we postulate that at the end of the active stage (approximately after $\tau_* \approx 80\%$ of the wave period), the layer thickens down to a maximum depth $k \cdot \bar{\delta}_{max}(\lambda) = 0.4$, in accordance with *Rapp and Melville's* [1990] measurements. Therefore the rate of vertical growth for the foam layer during stage A might be expressed as

$$\beta(\lambda) \simeq \frac{0.4}{k \cdot \tau_*} \simeq 9.9 \times 10^{-2} \lambda^{1/2}. \quad (6)$$

[31] The last parameter to be determined in equation (5) is the exponential time τ' . This parameter is the lifetime of (single) surface bubbles, and it differs for fresh and salt water samples. *Monahan and Zietlow* [1969] report τ' is 2.54 s for fresh water whitecaps and 3.85 s for salt water whitecaps. *Zheng et al.* [1983] show that the bubble lifetime follows a Rayleigh distribution. The mean lifetime is a function of the bubble size with average lifetimes of nominally 2.24, 2.98, and 3.89 s, reported of tap water, Delaware bay water, and Atlantic Ocean water, respectively. Accordingly, these measurements suggest $\tau' \approx 2.5$ s for fresh water and $\tau' \approx 3.8$ s for salt water. Note that these durations are not only due to how long the fresh- and salt-water bubbles persist once they reach the surface, but they also reflect the fact that these bubbles rise to the surface from the sub-surface bubble plume with different effective rise velocities, due in large measure to their different characteristic radii.

[32] Time evolution of the average vertical thickness of foam layers as a function of the breaker wavelength as predicted by the model (equation (5)) is illustrated in Figure 3. According to such a model, foam layers generated by breaking waves thicker than 5 cm only occur for underlying carrier wavelength greater than ≈ 1 m. Although our approach is an oversimplification of the actual unsteady flow, the most important physical features of transient breaking waves in the field should be included.

4. Models for the Incremental Breaking Statistics $\Lambda(\bar{c})$

4.1. $\Lambda(\bar{c})$: Definition

[33] The definition of the average length $\Lambda(\bar{c})$ of breaking fronts per unit area per unit speed interval has been originally introduced by *Phillips* [1985]. When a single breaking event starts, a turbulent foam patch is generally initiated at some point on the wave crest, and during the active breaking period, the patch spreads both laterally, along the direction of travel of the wave, and down into the water column. Although the foam patch area is turbulent

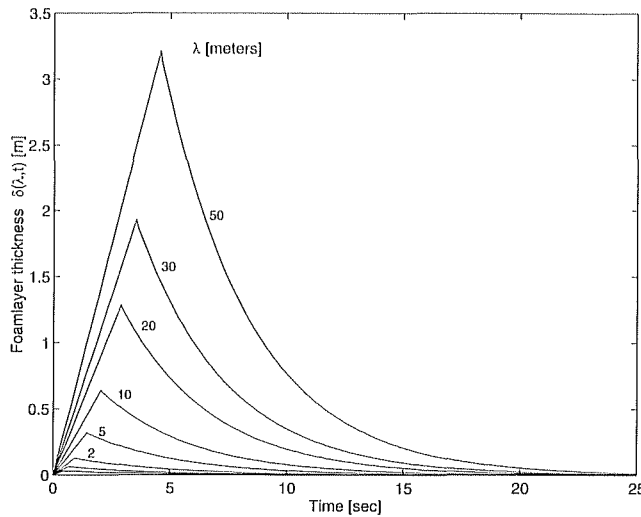


Figure 3. Evolution of the foam-layer thickness as a function of time for several breaking carrier wavelengths (number in meters) and for salt water ($\tau' = 3.8$ s).

and therefore exhibits intermittent boundaries during a complete breaking process, at any instant in time, its lateral dimension can always be represented by a main axis having the shape of an arc segment. The length of the breaking front Λ , at that particular time, is a measure of the length of this lateral arc segment (see Figure 2). As the wind blows over the water surface, at any instant, the fronts of the breaking waves therefore define a distribution of isolated lines or arc segments. The scales of the breaking waves cover a very wide range, from short gravity waves (15–30 cm or so) generating a very short-life turbulent patch with low air content, to actual whitecaps in which the breaking and the generation of turbulence is so vigorous that extensive patches of foam are generated.

[34] There is clearly some tight association of the foam patch initial dynamics and some characteristic scales of the carrying wave. *Phillips* [1985] proposed to use the velocity \vec{c} of the breaking fronts to parameterize their length. He introduced the distribution $\Lambda(\vec{c})$ [m^{-2} s], such that $\Lambda(\vec{c})d\vec{c}$ represents the average total length per unit surface area of breaking fronts that have velocities in the range \vec{c} to $\vec{c} + d\vec{c}$. The total length of breaking fronts per unit area is then

$$L = \int_0^{\infty} \int_{-\pi/2}^{\pi/2} \Lambda(\vec{c})d\vec{c}. \quad (7)$$

[35] In unit time, the fraction of sea-surface area traversed by breaking fronts with velocities between \vec{c} and $\vec{c} + d\vec{c}$ is $c\Lambda(\vec{c})d\vec{c}$, so that the fraction of total surface area turned over per unit time, or the turnover rate, is

$$R = \int_0^{\infty} \int_{-\pi/2}^{\pi/2} c\Lambda(\vec{c})d\vec{c}. \quad (8)$$

[36] This quantity also expresses the total number of breaking waves of all scales passing a given point per unit time; the distribution $c\Lambda(\vec{c})d\vec{c}$ specifies the expected num-

ber per unit time passing a fixed point with velocities in the interval \vec{c} to $\vec{c} + d\vec{c}$.

4.2. Model for $\Lambda(\vec{c})$ in a Sea State at Statistical Equilibrium

[37] The energy loss by an individual wave breaker was also quantified by [*Duncan*, 1981] during his experiments on quasi-steady breakers. The tangential force exerted per unit length by the weight of the breaking zone was found to be proportional to c^4/g with a proportionality factor equal to the previously introduced constant b , equation (4). The rate of energy loss D_{ind} per unit surface in a breaker moving with the phase speed c can therefore be expressed as

$$D_{ind}(c) = b(c^5/g). \quad (9)$$

Duncan's result is for quasi-steady breaking. *Melville* [1994] showed that similar scaling applies to unsteady breaking with a modified proportionality factor $b' \simeq (3-16) \cdot 10^{-3}$. The average value for unsteady breaker $b' \simeq 9 \cdot 10^{-3}$ is used further throughout the model calculations.

[38] On the basis of this formulation for the energy loss of an individual breaking wave, *Phillips* [1985] expressed the average rate of energy loss per unit area by breakers with speeds between \vec{c} and $\vec{c} + d\vec{c}$ as

$$\varepsilon(\vec{c})d\vec{c} = b'g^{-1}c^5 \Lambda(\vec{c})d\vec{c}. \quad (10)$$

[39] This average rate of energy loss by breakers per unit area, ε , can further be related in \vec{k} -space to the spectral rate of dissipation of wave action, namely the dissipation source term S_{ds} in the wave action balance equation,

$$\varepsilon(\vec{k})d\vec{k} = \omega S_{ds}(\vec{k})d\vec{k}, \quad (11)$$

where ω is the intrinsic frequency of the wave component with wavenumber in the range \vec{k} to $\vec{k} + d\vec{k}$. Thus, providing (1) a model for the dissipation source term S_{ds} and (2) a relationship between breaker lengths and velocities, equations (10) and (11) allow us to evaluate the total length of breaking fronts per unit area $\Lambda(\vec{c})$.

[40] There are several proposed forms for the dissipation source term $S_{ds}(\vec{k})$ [*Hasselmann*, 1974; *Komen et al.*, 1984; *Phillips*, 1985; *Donelan and Pierson*, 1987]. They were reviewed in detail by *Donelan and Yuan* in the work by *Komen et al.* [1994]. The modeling of the dissipation source function is the least understood aspect of the physics of wave evolution. Consequently, attempts to determine $\Lambda(\vec{c})$ from other and better known source functions, like the wind input source, seem preferable.

[41] Following *Phillips* [1985], a statistical equilibrium in the spectral gravity range will imply proportionality between all sources in the wave action balance. If $S_m(\vec{k})$ describes the wind input source function, in a sea state at statistical equilibrium, equation (11) can be rewritten [see *Phillips*, 1985, p. 522],

$$\varepsilon(\vec{k})d\vec{k} \propto \omega S_m(\vec{k})d\vec{k}. \quad (12)$$

[42] The input source function follows the standard definition,

$$S_{in}(\vec{k}) = \beta(\vec{k})N(\vec{k}), \quad (13)$$

with $\beta(\vec{k})$ being the wind input growth rate, and $N(\vec{k})$ the wave spectral action. From a survey of field and laboratory experiments, *Plant* [1982] suggests that the wind-induced wave growth rate is given by

$$\beta(\vec{k}) = m \left(\frac{u_*}{c} \right)^2 \cos(\theta)\omega, \quad (14)$$

where $m = (0.04 \pm 0.02)$, u_* is the wind friction velocity and θ the angle between the wind and the wave component \vec{k} . With the action spectral density defined as $N(\vec{k}) = gF(\vec{k})/\omega$, where $F(\vec{k})$ is the directional wavenumber spectrum of the sea surface, the average rate of energy loss by breakers per unit area, ε becomes

$$\varepsilon(\vec{k})d\vec{k} = m'g \left(\frac{u_*}{c} \right)^2 \cos(\theta)\omega F(\vec{k})d\vec{k}. \quad (15)$$

[43] In order to establish a model for $\Lambda(\vec{c})$, it is now necessary to relate breaker wavelengths to their speed. The use of the dispersion relation for deep water gravity waves $\omega = (gk)^{1/2}$ is valid only for waves free of any Doppler-shifting effects due to advection by the orbital velocities of longer waves. *Phillips* [1985] argued that Doppler shifting is insignificant for the components whose phase speeds $c > (2\pi s)C_p$, where C_p is the phase speed of the dominant wave and $s = \sqrt{\bar{\zeta}^2}/\lambda_p$ is the ‘‘significant slope,’’ defined as the ratio of the mean-square surface displacement in the wave field associated with the dominant wave to the wavelength at the peak of the surface wave spectrum. While care will be taken, we neglect Doppler-shifting effects for waves carrying whitecaps at a speed less than this threshold phase speed and apply the dispersion relationship even for the smaller breakers. However, we only consider waves longer than $\lambda_{min} = 20$ cm (with corresponding wavenumber $k_{max} = 2\pi/\lambda_{min}$), since waves shorter than this length generate capillaries rather than break to dissipate their energy [*Kudryavtsev et al.*, 1999]. Under these simplified assumptions, $k = g/c^2$, and, an element of area $d\vec{k}$ on the wavenumber plane can therefore be related to the element $d\vec{c}$ on the velocity plane by

$$d\vec{k} = -\frac{2g^2}{c^6}d\vec{c}. \quad (16)$$

[44] Combining equations (10), (15), and (16) yields the following expression for the distribution $\Lambda(\vec{c})$ for a sea-state at statistical equilibrium,

$$\Lambda_{eq}(\vec{c}) = -4b'^{-1}m'g^5c^{-14}u_*^2F(\vec{k})\cos(\theta), \quad (17)$$

where a factor 2 is arising since the direction of \vec{c} is taken to lie between $-\frac{\pi}{2}$ and $\frac{\pi}{2}$, while that of \vec{k} ranges over $-\pi$ to π .

[45] If the spectral model of *Phillips* [1985], $F(k) \propto \cos^{1/2}(\theta)u_*g^{-1/2}k^{-7/2}$ is chosen, $\Lambda(\vec{c}) \propto \cos^{3/2}(\theta)u_*^3gc^{-7}$ [see *Phillips*, 1985, equation (6.7)]. In the present work,

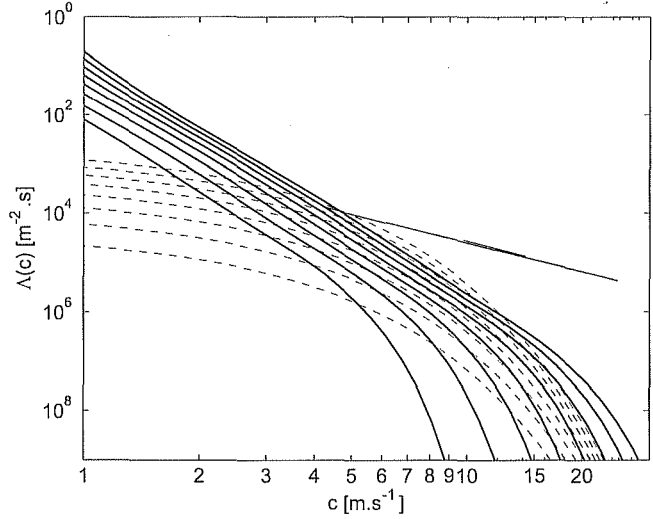


Figure 4. Omni-directional distribution of the length of breaking fronts at several wind speeds values, ranging from $U_{10} = 5$ to 19 m s^{-1} (by steps of 2 m s^{-1}). Thick lines: model for a sea state at statistical equilibrium; thin dotted lines: empirical model of *Melville and Matusov* [2002]; thin solid lines: model of *Makin and Kudryavtsev* [2002] for dominant breaking waves.

we use for $F(\vec{k})$ the empirically derived unified spectral model of *Elfouhaily et al.* [1997] because it reproduces well significant wave height for developing seas and measured mean square slopes. Finally, the evolution of the omni-directional distribution of breaking front length can be written

$$\Lambda_{eq}(c) = \int_{-\pi/2}^{\pi/2} c \Lambda_{eq}(\vec{c})d\theta, \quad (18)$$

and is shown in Figure 4 for different wind speeds using the unified spectral model for fully developed seas (inverse wave age is set to 0.8).

4.3. Empirical Model of $\Lambda(\vec{c})$

[46] Recently, *Melville and Matusov* [2002] were able to measure the distribution function $\Lambda(\vec{c})d\vec{c}$ from video images acquired from a light aircraft. Using a particle imaging velocimetry technique (PIV), they could measure the velocity of the local boundary of individual whitecaps, giving $\Lambda(\vec{c})d\vec{c}$. Data collected at three averaged 10-m wind speeds ($U_{10} = 7.2, 9.8$ and 13.6 m s^{-1}) for well-developed sea-states (wind-wave fetch was in the range 100–150 km) shows that when weighted by U_{10}^{-3} , the measurements of $\Lambda(c)$ collapse approximately onto a single exponential curve,

$$\Lambda_{emp}(c) = (U_{10}/10)^3 \times 3.3 \times 10^{-4} e^{-0.64c}. \quad (19)$$

[47] Figure 4 compares the results from *Melville and Matusov's* [2002] empirical fit to the previous model for a fully developed sea state at statistical equilibrium. As noticed by *Melville and Matusov* [2002], their empirical results are consistent with *Phillips's* [1985] equilibrium

subrange for larger c values where $\Lambda(c) \propto c^{-6}$ locally in both cases. However, at small c values, the model of $\Lambda(c)$ for a fully developed sea state at statistical equilibrium predicts a much higher density of small breakers than the one measured by *Melville and Matusov* [2002].

4.4. Statistical Model of $\Lambda(\bar{c})$ for Dominant Waves

[48] Models for ocean wave breaking statistics usually share the common hypotheses that wave breaking occurs when some random variable describing the wave field exceeds a critical value. Among the various physical parameters describing the field, the variables most often associated with wave breaking criteria are the surface elevation [*Longuet-Higgins*, 1969; *Huang et al.*, 1986], the horizontal velocity [*Banner and Phillips*, 1974; *Liu and Yan*, 1995], the vertical acceleration [*Kennedy and Snyder*, 1983; *Srokosz*, 1986], and the surface slope [*Ochi and Tsai*, 1983; *Longuet-Higgins*, 1987; *Banner et al.*, 2000].

[49] *Makin and Kudryavtsev* [2002] proposed a model of $\Lambda(\bar{c})$ for dominant waves that is based on a statistical concept of a threshold level for surface elevation. They used a general expression for the mean length of a contour represented by the intersection of the wavy surface by a plane of a constant height $\zeta = \zeta_0 = \text{const}$ per unit area, as derived by *Longuet-Higgins* [1957] for a narrow band process. When the surface level ζ exceeds the threshold level ζ_0 , waves are assumed to break. The average total length per unit surface area of breaking fronts can then be found from the length of contours at that level.

[50] Assuming the dominant wave spectrum to be narrow, *Makin and Kudryavtsev* [2002] proposed the following form for $\Lambda(\bar{c})$ which should only be valid in the wavenumber range $k \leq 2k_p$, where k_p is the spectral peak wavenumber:

$$\Lambda_{dom}(\bar{c})d\bar{c} = \frac{1}{2\pi} k \exp\left(-\frac{\varepsilon_T^2}{\varepsilon_s^2}\right), \quad (20)$$

where $\varepsilon_s = 2k_m m_{00}^{1/2}$ is the dominant wave steepness, $k_m = (m_{20}/m_{00})^{1/2}$ defines the mean wavenumber, and $m_{mn} = \int k_x^m k_y^n F(k) d\vec{k}$ are the spectral moments of order mn . In equation (20), $\varepsilon_T = \sqrt{2}\zeta_0 k_m$ is a tuning constant. Using $\varepsilon_T = 0.24$, *Makin and Kudryavtsev* [2002] found good agreement between their model and measurements by *Banner et al.* [2000]. This value is used for the model calculations.

[51] Using the unified spectral model to calculate the spectral moments m_{00} and m_{20} , we plot in Figure 4 the omni-directional distribution of breaking front lengths for dominant waves as given by *Makin and Kudryavtsev's* [2002] model. It is calculated only for breaking fronts with speeds ranging from c_p , the speed at the peak of the wave spectrum, to $c = \sqrt{2g/k_p}$. For all breaking front speeds within this range, *Makin and Kudryavtsev's* [2002] model exhibits a significantly larger average length of breaking fronts than both the empirical model and the one for sea state at statistical equilibrium.

5. Total Whitecap Coverages

5.1. Model for the Time of Persistence of the Foam Layers

[52] The persistence time τ of a foam layer, once generated, can be defined as the time at which its thickness

becomes infinitesimal. According to our dynamical model for $\bar{\delta}(\lambda, t)$, this limit depends on the scale of the underlying carrier wave (see Figure 3). Therefore, for an individual breaker, the persistence time of the generated foam layer is proportional to the period of the underlying carrier wave: $\tau = a \cdot T_b = a \cdot 2\pi c/g$, where a is a constant of proportionality. If the foam-layer persistence time τ is chosen to be less than the active breaking event duration $\tau_{*} = 0.8 \cdot T_b$, i.e., if $a \leq 0.8$, only “dynamic-foam”-type formations (Stage A breakers) are taken into account for the whitecap coverage deduced from equation (3). For $a > 0.8$, only static-foam-type is included in the coverage model.

5.2. Comparison With Semi-Empirical Fits

[53] With $\tau = a2\pi c/g$, equation (3) can be rewritten as a function of the omni-directional distribution of breaking fronts length $\Lambda(c, U)$ as follows:

$$F(U) = \frac{2a\pi}{g} \int_{c_{min}}^{c_p} c^2 \Lambda(c, U) dc, \quad (21)$$

where the integration is restricted to waves faster than $c_{min} = (g\lambda_{min}/2\pi)^{1/2}$ and slower than the phase speed at the peak of the wave spectrum c_p .

[54] To validate our dynamical model for F , numerical results given by equation (21) using previously described models for $\Lambda(c, U)$ can be compared to the most popular reported semi-empirical algorithms. It is commonplace to fit the wind-speed-dependent whitecap coverage to the power-law, such as

$$F = \alpha U_{10}^\beta, \quad (22)$$

where α and β are constants and U_{10} is the wind speed at the reference height 10 m. On the basis of photographic images collected from low-altitude ship platforms, *Monahan and O'Muircheartaigh* [1980] proposed

$$F = 3.84 \times 10^{-6} U_{10}^{3.41}. \quad (23)$$

Bondur and Sharkov [1982] used airborne platform high-resolution photographic imagery to separate and quantify the two following phenomena: (1) fresh dense foam patches from breaking waves and (2) low-reflectance residual foam layers. On the basis of the shape and brightness of whitecap images, they divide the whitecap formations into crests of dynamic foam and striplike or patchy structure of static foam with lifetimes on the order of a few seconds to many seconds, respectively. The first stage (Stage A according to *Monahan classification*) is most closely associated with the spilling breaker (α -plume) which forms a small but highly reflective foam patch and the second stage (resp. Stage B) is associated with the evolving foam layer (transient entrained bubbles and surface-bubble decay: β , γ -plumes). *Bondur and Sharkov* [1982] proposed

$$F = 6.5 \times 10^{-3} \left[1 + 4.76 \times 10^{-2} (U_{10} - 5)^2 \right] \quad (\text{static foam})$$

$$F = 1.5 \times 10^{-4} \left[1 + 2.2 \times 10^{-2} (U_{10} - 5)^3 \right] \quad (\text{crest foam}).$$

(24)

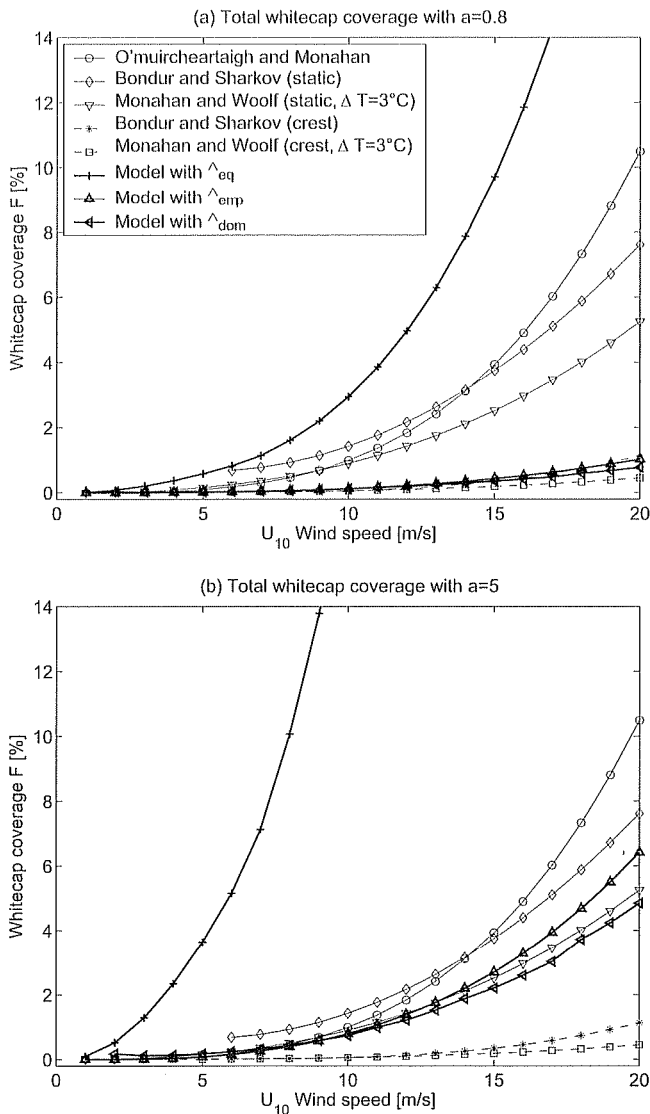


Figure 5. Comparison between empirical fits of whitecap coverage as a function of wind speed for dynamic and static foam and the dynamical model. (a) Persistence time of foam τ is chosen equal to active breaking event durations τ_* . (b) Here τ is chosen equal to 5 times the underlying carrier wave periods.

The static-foam law (equation (24)) is used in the emissivity model developed by *Kunkee and Gasiewski* [1997].

[55] These properties were also quantified in a similar way by *Monahan and Woolf* [1989]. They processed video images using brightness discrimination level and proposed

$$F = 1.95 \times 10^{-5} U_{10}^{2.5} \exp(0.0861 \Delta T) \quad (\text{static foam})$$

$$F = 2.92 \times 10^{-7} U_{10}^{3.204} \exp(0.198 \Delta T) \quad (\text{crest foam}). \quad (25)$$

These correlations include departures from thermal equilibrium, $\Delta T = T_{sea} - T_{air}$ (deg C). Their conclusions agree with those of *Bondur and Sharkov* [1982]. Whitecap coverage by the post wave-breaking foam layer represents 80–85% of the total whitecap coverage in the visible.

[56] As illustrated in Figure 5, if a is taken equal to 0.8 with the empirical model of *Melville and Matusov* [2002] for the

distribution function $\Lambda(c)$, the whitecap coverage model given by equation (21) agrees very well with the empirical laws of “crest-foam” coverage. The curve predicted by the model fits closely *Bondur and Sharkov*'s [1982] law and lies at a slightly higher level than *Monahan and Woolf*'s [1989] fit if a value of $\Delta T = 3^\circ\text{C}$ is chosen (the significance of this parameter will be discussed further). If the model $\Lambda_{eq}(c)$ for sea states at statistical equilibrium is used in equation (21) with $a = 0.8$, the modeled foam coverage dependence with wind speed is significantly higher than the reported whitecap coverage for static foam. Since for $a \leq 0.8$, only crest-foam formations should be accounted for, the model clearly overestimates the whitecap coverage. When the model $\Lambda_{dom}(c)$ is used, the foam coverage is also found to correctly reproduce the reported foam-crest coverages.

[57] Good agreement is also found between the model using $\Lambda_{emp}(c)$ in equation (21) and the empirical data for static-foam coverage with $a \sim 5$. This numerical value reflects the fact that reported total static-foam coverage should correspond to the sum of individual sea surface area swept by each breaking front during approximately five wave periods.

[58] For that particular value of a , $\Lambda_{eq}(c)$ and $\Lambda_{dom}(c)$ are, respectively, overestimating and underestimating the reported foam coverages. However, the model for $\Lambda_{dom}(c)$ indicates that a significant fraction of the sea surface covered by static foam is generated by dominant breaking waves.

6. Conditional Whitecap Coverages

[59] To determine the conditional sea surface area covered by Foam layers having a given thickness $\bar{\delta}$, the dynamical model for individual whitecap thickness $\bar{\delta}(\lambda, t)$ and the model for overall whitecap coverage $F(U)$ must be connected. The idea is to associate a given class of breaking fronts moving at speed between c and $c + dc$ with a characteristic foam-layer thickness. Given the distribution $\Lambda(c, U)$, there is equiprobability for individual foam layers to be in any configuration between incipient growth and the end stages of the foaming process. A characteristic whitecap thickness scale for the class of breaking fronts moving at speed between c and $c + dc$ can thus be defined as

$$\bar{\delta}_\tau(c) = \langle \delta(c) \rangle_\tau = \frac{1}{\tau} \int_0^\tau \Pi(t) \cdot \bar{\delta}(\lambda, t) dt, \quad (26)$$

where $\Pi(t) = 1$ for $0 \leq t \leq \tau$ is the probability for a whitecap to be at a particular stage of evolution during the foam-layer persistence duration τ . The characteristic thickness scale $\bar{\delta}_\tau(c)$ represents the most probable time-averaged thickness of foam layers generated by breakers moving at speed between c and $c + dc$, during the period of observation τ .

6.1. Thickness Distribution for the Crest-Foam Coverage

[60] According to equations (26), (5), and (6), the characteristic thickness of dynamic-foam patches ($a = 0.8$) generated by breakers moving at speed between c and $c + dc$ is given by

$$\bar{\delta}_{\tau*}(c) = \frac{0.4}{2k} = \frac{0.4c^2}{2g}. \quad (27)$$

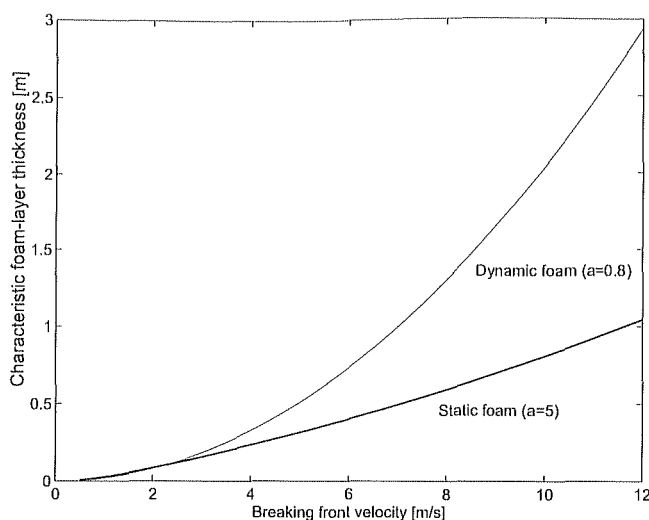


Figure 6. Characteristic foam-layer thickness scale as a function of the carrier breaking wave velocity. Thin line: crest-foam characteristic thickness (see equation (27)); thick line: static foam characteristic thickness (see equation (30)) if $a = 5$.

The evolution of $\bar{\delta}_{\tau^*}(c)$ with c is plotted in Figure 6. Using equation (27), an increment of foam-layer thickness $d\bar{\delta}_{\tau^*}$ can be related to an increment of breaking front velocity dc . The incremental crest-foam coverage associated with foam layers having thicknesses between $\bar{\delta}_{\tau^*}$ and $\bar{\delta}_{\tau^*} + d\bar{\delta}_{\tau^*}$ is therefore the one associated with breaking front velocities between c and $c + dc$,

$$dF_c(U, \bar{\delta}_{\tau^*}) = \frac{1.6\pi}{g} c^2 \wedge(c, U) dc. \quad (28)$$

[61] For the empirical expression \wedge_{emp} , the incremental crest-foam fractional coverage due to foam layers with thickness between $\bar{\delta}_{\tau^*}$ and $\bar{\delta}_{\tau^*} + d\bar{\delta}_{\tau^*}$ is expressed as follows:

$$dF_c(U_{10}, \bar{\delta}_{\tau^*}) \simeq 2.9 \times 10^{-5} U_{10}^3 \sqrt{\bar{\delta}_{\tau^*}} e^{-4.48 \sqrt{\bar{\delta}_{\tau^*}}} d\bar{\delta}_{\tau^*}. \quad (29)$$

[62] In Figure 7, we plot the integration of $dF_c(U_{10}, \bar{\delta}_{\tau^*})$ from the lower characteristic thickness limit $\delta_{min} \simeq 7$ mm (which corresponds to the minimum breaking front velocity: $\delta_{min} = 0.4c_{min}^2/2g$) to a varying upper limit $\bar{\delta}_{lim}$. The model predicts that at least two thirds of the sea surface covered by crest foam in fully developed seas is due to air-water mixture patches thinner than 60 cm, whatever wind speed conditions.

6.2. Thickness Distribution for the Static-Foam Coverage

[63] To evaluate the thickness distribution for the static-foam coverage, the persistence time τ of foam layers needs to be set at larger values than the breaking event duration τ^* , i.e., $a \geq 0.8$. In this case, the characteristic thickness of static-foam patches generated by breakers moving at speed between c and $c + dc$ can be derived from equations (26), (5), and (6),

$$\bar{\delta}_{\tau}(c) = \frac{0.4c}{2\pi a} \left[\frac{5c}{2g} + \tau' \left(1 - e^{-\frac{c}{\tau'(2\pi a - 5)}} \right) \right]. \quad (30)$$

This model for $\bar{\delta}_{\tau}(c)$ is compared to the characteristic thickness scale for crest-foam layers in Figure 6. As expected from our assumptions, foam layers are always thicker on average during the active stage of breaking.

[64] The incremental static-foam coverage associated with foam layers having thicknesses between $\bar{\delta}_{\tau}$ and $\bar{\delta}_{\tau} + d\bar{\delta}_{\tau}$ is the coverage associated with breaking fronts with velocities between c and $c + dc$ after a duration τ ,

$$dF_s(U, \bar{\delta}_{\tau}) = \frac{2a\pi}{g} c^2 \wedge(c, U) dc. \quad (31)$$

It can be numerically evaluated with the empirical expression \wedge_{emp} and with $a = 5$. In Figure 8, we plot the integration of $dF_s(U_{10}, \bar{\delta}_{\tau})$ from the lower characteristic thickness limit $\delta_{min} = 1$ mm to a varying upper limit $\bar{\delta}_{lim}$. The model predicts that at least two thirds of the sea surface covered by static foam in fully developed seas is due to air-water mixture patches thinner than 35 cm, whatever wind speed conditions. According to the model, approximately all the coverage is due to layers thinner than 1 m.

6.3. Effects of the Atmospheric Boundary-Layer Stability

[65] As shown in Figure 9, if the temperature difference between air and water increases from 0°C to 10°C, the empirical laws derived by Monahan and Woolf [1989] reveal that the fractional coverage due to crest foam increases by about a factor of 8. A weaker thermal effect was found by Monahan and Woolf [1989] on the fractional coverage of static-foam formations. Still, an increase of 10°C in ΔT approximately corresponds to an increase of the static-foam coverage by 3 (see Figure 10b).

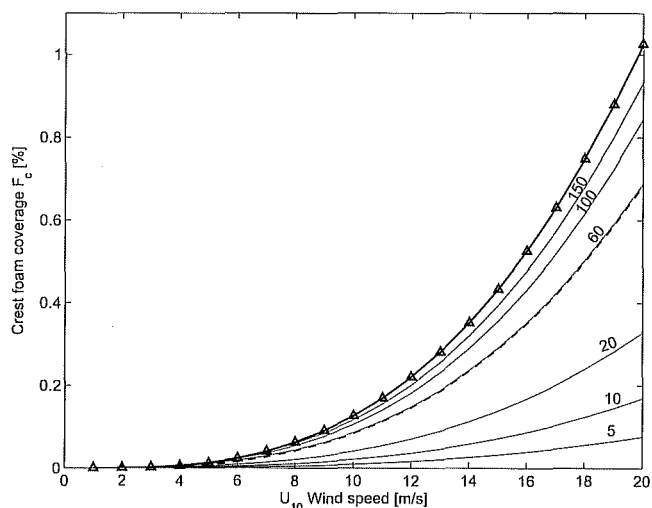


Figure 7. Fractional surface coverage of crest foam associated with layers thinner than a threshold value $\bar{\delta}_{lim}$, given numerically in centimeters above each curve. The thick line with triangles is the total crest-foam fractional coverage deduced from the model with $\wedge = \wedge_{emp}$ and $a = 0.8$. The dashed lines represents two thirds of that coverage.

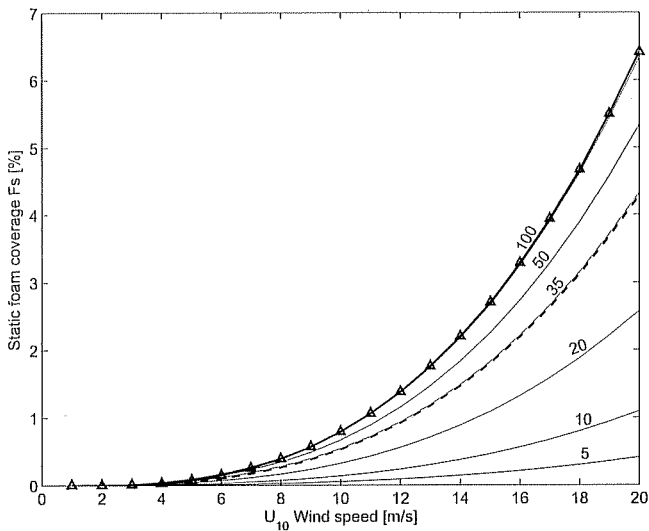


Figure 8. Fractional surface coverage of static foam associated with layers thinner than a threshold value $\bar{\delta}_{lim}$, given numerically in centimeters above each curve. The thick line with triangles is the total static-foam fractional coverage deduced from the model $\Lambda = \Lambda_{emp}$ and $a = 5$. The dashed lines represents two thirds of that coverage.

[66] This important effect is not dynamically taken into account in our model. An empirical correction factor for atmospheric stability impact is therefore introduced as follows:

$$F(U) = \frac{2a\pi}{g} \left[\int_{c_{min}}^{c_p} c^2 \Lambda(c, U) dc \right] \times e^{(\alpha\Delta T - \beta)}, \quad (32)$$

where the parameters α and β of the thermal correction factor are determined for both crest foam and static foam by best fitting the model to *Monahan and Woolf's* [1989]

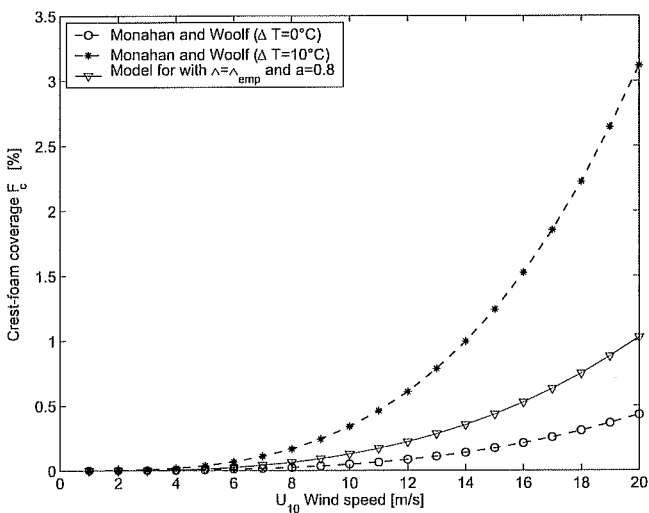


Figure 9. Effects of the boundary-layer stability parameter ΔT on the crest-foam coverage as reported by *Monahan and Woolf* [1989].

empirical laws (equation (25)). Using a least-square method, the determined numerical values for α and β are

$$\begin{cases} \alpha_c = 0.198 \\ \beta_c = 0.91 \end{cases} \quad \text{for crest-foam coverage and,} \quad (33)$$

$$\begin{cases} \alpha_s = 0.0861 \\ \beta_s = 0.38 \end{cases} \quad \text{for static-foam coverage.}$$

[67] Efficiency of the added empirical correction factors is illustrated in Figure 10. The model correctly reproduces the wind speed dependence for crest-foam coverage as a function of ΔT . For the static-foam coverage, differences are, however, generated by the use of a power 3 dependence with the wind speed U_{10} in the model for Λ_{emp} , in contrast to a power 2.55 dependence in *Monahan and Woolf's* [1989] empirical laws (equation (25)).

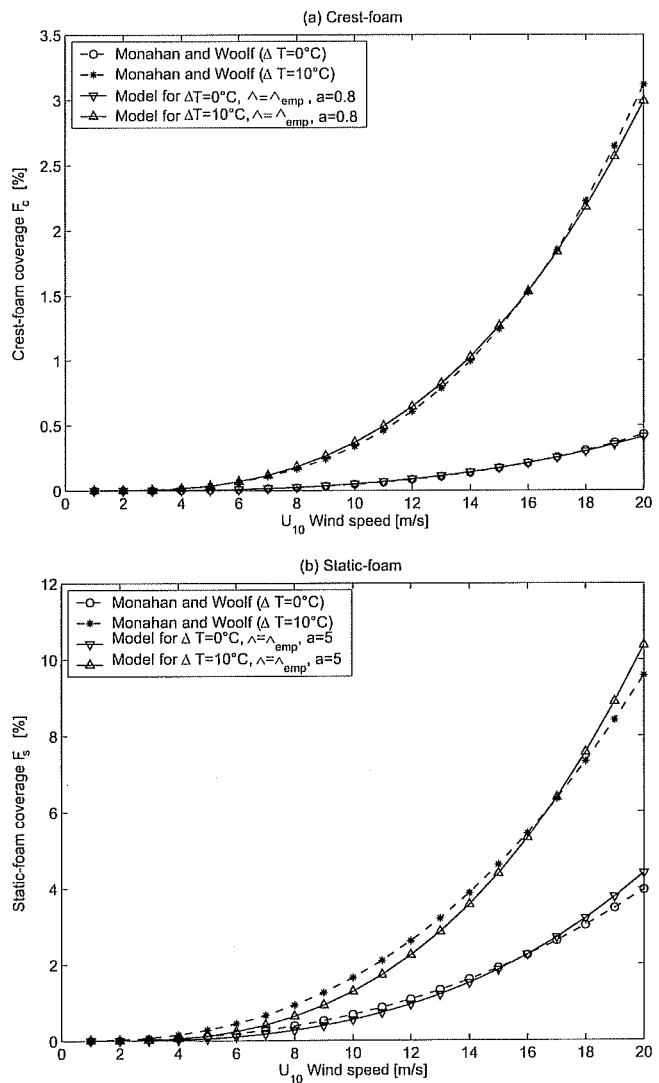


Figure 10. Effects of the thermal stability correction factors on (a) the crest-foam coverage model and (b) the static-foam coverage model.

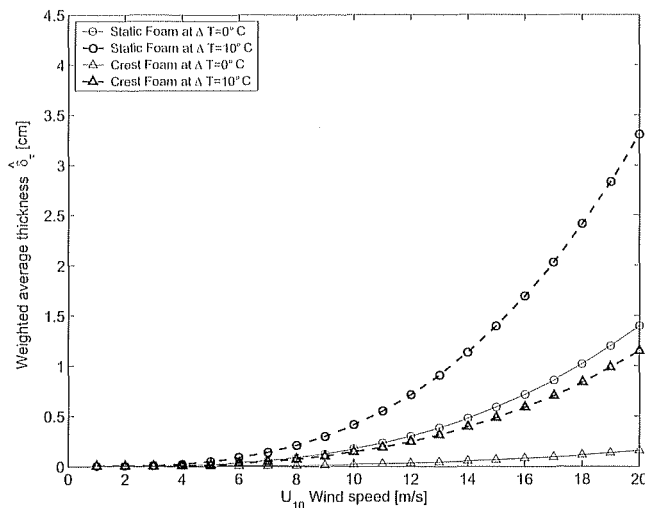


Figure 11. Coverage-weighted average foam-layer thickness.

[68] The previously determined incremental crest-foam and static-foam coverages associated with foam layers having thicknesses between $\bar{\delta}_\tau$ and $\bar{\delta}_\tau + d\bar{\delta}_\tau$ can now be simply corrected for the thermal effects by respectively multiplying equations (29) and (31) by the correction factors $e^{(\alpha_c \Delta T - \beta_c)}$ and $e^{(\alpha_s \Delta T - \beta_s)}$.

6.4. Average Thickness as a Function of Wind Speed

[69] An interesting parameter in the context of the present model is the foam-layer thickness weighted by the corresponding conditional surface foam coverage and averaged over all breaking wave scales for a given wind speed,

$$\hat{\delta}_\tau(U_{10}) = \int_{\delta_{min}}^{\delta_p} \bar{\delta}_\tau \cdot dF(U_{10}, \bar{\delta}_\tau). \quad (34)$$

[70] It is plotted as a function of U_{10} for crest foam and static foam in Figure 11. It can be seen that the globally averaged foam-layer thickness weighted by the coverage is less than 3.5 cm for static foam and less than 1 cm for crest foam. As expected, the stronger the wind speed, the thicker the layers on average. Although crest-foam layers associated with a given scale of breaking waves are thicker than the subsequent static patches, $\hat{\delta}$ is smaller for crest-foam than for static-foam formations due to smaller fractional coverage. This parameter is directly related to the overall impact of the Foam thickness on the microwave brightness signatures as a function of wind speed.

7. Conclusions and Discussion

[71] A bibliographical survey on the microwave emissivity of sea-foam formations was conducted and highlighted the fact that small variations in the thickness of individual foam layers strongly influence the amount of emitted microwave radiations. The thickness of foam layers generated by breaking waves is naturally distributed due to the large range of surface wave scales involved in the breaking process at sea and because of the basic unsteadiness of the phenomenon. The overall microwave brightness due to

foam formations in a given sea surface area is therefore the sum of individual contributions from several foam patches with varying thicknesses. Although the effects of a distributed thickness parameter on the foam-induced brightness temperature may have an intensity comparable to, and even in some cases larger than, the fractional whitecap coverage, it is not yet included in brightness temperature models. To fill this gap, we developed a dynamical model for the conditional fraction of sea surface covered by foam layers with thicknesses between $\bar{\delta}$ and $\bar{\delta} + d\bar{\delta}$, as a function of the wind speed at 10-m height U_{10} .

[72] The thickness of an individual foam layer was defined here as the depth at which air bubbles and turbulence are injected into the water column. In the available electromagnetic emissivity models for foam [e.g., *Ulaby et al.*, 1986; *Dombrovskiy and Raizer*, 1992; *Guo et al.*, 2001], sea-foam layers are often described as layers of air-water mixture with clearly defined lower boundaries between the foam media and the underlying water masses. The basic assumption in these models is that the whitecap can be regarded as a distinct turbulent flow that traps enough air bubbles for the resulting air-water mixture to be lighter than the water below. If the density difference inhibits mixing with the wavy water interface, the foam layer might be assumed to ride on the top of the water surface. As shown by *Longuet-Higgins and Turner* [1974], such a model of "above the surface foam" is relevant to quasi-steady breaking for which the foam layer retains its overall identity during the process.

[73] However, underwater measurements of the evolution of turbulent bubbles clouds generated just underneath unsteady breakers [e.g., *Rapp and Melville*, 1990] reveal that the vertical downward extent of the foam-layer is basically unsteady. In particular, *Rapp and Melville's* [1990] measurements show that the depth of injection of the turbulent air-water patches into the water column is driven by the scale of the carrier wave within breaking wave groups, and the depth exhibits a fast monotonic growth during the active stage of breaking. Similarly, reported temporal evolutions of visual surface signatures of individual unsteady whitecaps also show a fast monotonic growth of whitecap boundaries during the active stage of breaking followed by a slower exponential decay. Assuming a self-similarity between the foam-layer dynamics in the horizontal and vertical planes, we combined these existing experimental results to provide a consistent time-dependent model $\bar{\delta}(\lambda, t)$ for the thickness of foam layers generated by individual breaking waves with length scale λ . In the context of foam-emissivity modeling, it is important to stress that the vertical distribution $\nu(z, \lambda, t)$ of the air void fraction within a foam layer with thickness described by $\bar{\delta}(\lambda, t)$ is certainly not constant at any instant t . At the air/foam interface, air void fraction is indeed 1 and the lower boundary of the layer is by definition located at a depth at which air void fraction is zero. Although it is out of the scope of the present paper, a model for the void fraction vertical distribution within foam layers as a function of the scale of breaking waves $\nu(z, t, \lambda) = \nu(z/\bar{\delta}(\lambda), t)$ is also needed.

[74] A key parameterization in our dynamical model of foam coverage is the distribution $\Lambda(\vec{c})d\vec{c}$ of the total length of breaking fronts moving with speed between \vec{c} and $\vec{c} + d\vec{c}$. The modeled function $\Lambda_{eq}(\vec{c})$ derived from *Phillips'* [1985]

analysis for sea states at statistical equilibrium provides a direct relationship between the average total length of breaking fronts of a given scale and the corresponding wave-height spectral level (see equation (17)). It is beyond the scope of the present paper to discuss whether a given scale of breaking wave (velocity, wavenumber) is uniquely associated with the spectral level at that same scale. However, it has long been pointed out that dynamical and statistical characteristics of wave breaking events, as localized discontinuities, will imply signatures over a wide spectral range [Rapp and Melville, 1990; Meza et al., 2000]. Consequently, it may be understood that $\Lambda_{eq}(\bar{z}, U)$ is somehow overestimated for the shortest scales. It is also expected that $\Lambda_{eq}(\bar{z}, U)$ will not apply for the dominant scales near the spectral peak. For this region a statistical model as derived by Makin and Kudryavtsev [2002] is certainly more pertinent. However, the most consistent parameterizations for the whitecap coverage are obtained when considering the experimentally derived form for $\Lambda_{emp}(\bar{z}, U)$ proposed by Melville and Matusov [2002]. Using their proposed distribution, a mean persistence time $\tau \simeq 0.87\tau_b$ for foam layers, consistent with reported active breaking event durations, well reproduces the empirical laws of crest-foam coverage. Considering large persistence time, our model predictions also match the empirical laws of static-foam coverage when a proportionality factor of 5 is chosen between persistence time and breaking wave periods. This duration is slightly longer than the one reported by Rapp and Melville [1990], who found a maximum depth of bubble injection after four wave periods. However, the greater numerical value we found in order to match empirical fits can be understood since static-foam formations are not solely generated by breaking waves but also by Langmuir circulation (e.g., foam streaks), and this is not included in our model. Moreover, when the persistence time τ is artificially set at larger values than the active breaking time in our modeling, motion is attributed to the whitecap after the wave had stopped breaking. Common observation suggests that the foam clouds progressively loose their advection velocity after the active breaking period: Consequently, our whitecap coverage model for static foam provides an approximate description of the real long-lived foam clouds.

[75] Following this development, a conditional foam coverage $F(U, \bar{\delta})$ of foam formations with thickness $\bar{\delta}$ was consistently determined. Empirical corrections to account for atmospheric boundary-layer stability were also added. As expected, our model predicts that foam layers are on average thicker with wind speed. When air-sea temperature difference is about 10°C , we found that foam-layer thicknesses reach maximum averaged value at $U = 20$ m/s of about 4 cm and 1 cm for static- and crest-foam formations, respectively. These values are approximately divided by two in neutral conditions. To our knowledge, there is no available experimental data to validate the model results. However, they are consistent with Wilheit's [1979] estimate of an overall averaged sea foam-layer thickness of 1 cm. Indeed, the apparent microwave brightness temperature of the sea surface due to foam has long been known to be dominantly determined by spilling wave crests (or stage A whitecaps) and not static foam [see e.g., Wang et al., 1995; Monahan, 2002]. The numerical value deduced by Wilheit

[1979] from data collected by satellite-borne microwave radiometers is therefore consistent with our model predictions for crest foam.

[76] According to emissivity models and measurements, saturation in foam emissivity, i.e., foam radiations tending to that of a black body, occurs only if sea-foam thickness is larger than about 2 times the electromagnetic wavelength. Our model predicts that no saturation should be observed on average for microwave frequencies from Ku-Band (1.7–2.5 cm) to L-band (15–30 cm) at wind speeds smaller than 20 m/s. Saturation might, however, appear for smaller wavelengths such as the Ka-Band (0.75–1.2 cm) either when the wind speed is greater than about 14 m/s and the air-sea temperature difference is about 10°C , or for $U > 18$ m/s in neutral stability conditions. According to our model, under neutral conditions, an increase in wind speed from 0 to 20 m/s induces a 2-cm increase for the average sea-foam thickness. This will approximately induce doubling of foam emissivity at Ku and C bands measurements according to theoretical calculations by either Bordonskiy et al. [1978], Droppleman [1970], or Guo et al. [2001].

[77] Since bubble void fractions and size distributions beneath breaking waves also depend on the breaking wave scales, the present model can also be extended to estimate the integrated evolution of these parameters with wind speed. In the near future, the proposed set of parameterizations will then be used, in conjunction with emissivity models, to better assess the impact of breaking waves on the measured brightness temperature. As foreseen, this will facilitate the development of a consistent inversion of sea surface characteristics (wind stress, gas transfer coefficient, etc.) and breaking wave statistics [see, e.g., Anguelova, 2002] from passive microwave measurements at differing frequencies.

[78] **Acknowledgments.** This work was supported by the European Space Agency under contract 14273/00/NL/DC. We are very grateful to reviewers for valuable comments and corrections and personally thank Kendall Melville for useful criticism of the manuscript.

References

- Anguelova, M., Whitecaps, sea-salt aerosols, and climate, Ph.D. thesis, Grad. Coll. of Mar. Stud., Univ. of Del., Lewes, Del., 2002.
- Asher, W., Q. Wang, E. C. Monahan, and P. M. Smith, Estimation of air-sea gas transfer velocities from apparent microwave brightness temperature, *Mar. Technol. Soc. J.*, 32, 32–40, 1998.
- Banner, M. L., and O. M. Phillips, On the incipient breaking of small-scale waves, *J. Fluid Mech.*, 65, 647–656, 1974.
- Banner, M. L., A. V. Babanin, and I. R. Young, Breaking probability for dominant waves on the sea surface, *J. Phys. Oceanogr.*, 30, 3145–3160, 2000.
- Barber, R. P., and J. Wu, Sea brightness temperature effects of spray and whitecaps, *J. Geophys. Res.*, 102, 5823–5827, 1997.
- Bondur, V. G., and E. A. Sharkov, Statistical properties of whitecaps on a rough sea, *Oceanology*, 22, 274–279, 1982.
- Bordonskiy, G. S., I. B. Vasil'kova, N. N. V. V. M. Veselov, Y. A. Militkiy, V. G. Mirovskiy, V. N. Nkitin, V. Y. Raizer, Y. B. Khapin, Y. A. Sharkov, and V. S. Etkin, Spectral characteristics of the emissivity of foam formations, *Izv. Atmos. Oceanic Phys.*, 14, 464–469, 1978.
- Bortkovskii, R., *Air-Sea Exchange of Heat and Moisture During Storms* (rev. Engl. vers.), D. Reidel, Norwell, Mass., 1987.
- Dombrovskiy, L. A., Calculation of the thermal radiation emission of foam on the sea surface, *Izv. Atmos. Oceanic Phys.*, 15, 193–198, 1979.
- Dombrovskiy, L. A., and V. Y. Raizer, Microwave model of a two-phase medium at the ocean surface, *Izv. Atmos. Oceanic Phys.*, 28, 650–656, 1992.
- Donelan, M., and W. Pierson, Radar scattering and equilibrium ranges in wind-generated waves with application to scatterometry, *J. Geophys. Res.*, 92, 4971–5029, 1987.

- Droppleman, J. D., Apparent microwave emissivity of sea foam, *J. Geophys. Res.*, 75, 696–698, 1970.
- Duncan, J., An experimental investigation of breaking waves produced by a towed hydrofoil, *Proc. R. Soc. London, Ser. A*, 377, 331–348, 1981.
- Elfouhaily, T., B. Chapron, K. Katsaros, and D. Vandemark, A unified directional spectrum for long and short wind-driven waves, *J. Geophys. Res.*, 102, 15,781–15,796, 1997.
- Guo, J., L. Tsang, W. Asher, K.-H. Ding, and C.-T. Chen, Applications of dense media radiative transfer theory for passive microwave remote sensing of foam covered ocean, *IEEE Trans. Geosci. Remote Sens.*, 39, 1019–1027, 2001.
- Hasselmann, K., On the spectral dissipation of ocean waves due to whitecapping, *Boundary Layer Meteorol.*, 6, 107–127, 1974.
- Huang, N. E., L. F. Bliven, S. R. Long, and C.-C. Tung, An analytical model for oceanic whitecap coverage, *J. Phys. Oceanogr.*, 16, 1597–1604, 1986.
- Kennedy, R. M., and R. L. Snyder, On the formation of whitecaps by a threshold mechanism: II. Monte carlo experiments, *J. Phys. Oceanogr.*, 13, 1493–1504, 1983.
- Koepke, P., Effective reflectance of oceanic whitecaps, *Appl. Opt.*, 23, 1816–1824, 1984.
- Koepke, P., Remote sensing signatures of whitecaps, in *Oceanic Whitecaps, and Their Role in Air-Sea Exchange Processes*, edited by E. C. Monahan and G. MacNiocaill, pp. 251–260, D. Reidel, Norwell, Mass., 1986a.
- Koepke, P., Oceanic whitecaps: Their effective reflectance, in *Oceanic Whitecaps, and Their Role in Air-Sea Exchange Processes*, edited by E. C. Monahan and G. MacNiocaill, pp. 272–274, D. Reidel, Norwell, Mass., 1986b.
- Komen, G. J., S. Hasselmann, and K. Hasselmann, On the existence of a fully developed wind-sea spectrum, *J. Phys. Oceanogr.*, 14, 1271–1285, 1984.
- Komen, G. J., L. Cavaleri, M. Donelan, K. Hasselmann, S. Hasselmann, and P. A. Janssen, *Dynamics and Modelling of Ocean Waves*, Cambridge Univ. Press, New York, 1994.
- Kudryavtsev, V. N., V. K. Makin, and B. Chapron, Coupled sea surface-atmosphere model: 2. Spectrum of short wind waves, *J. Geophys. Res.*, 104, 7625–7639, 1999.
- Kunke, D. B., and A. J. Gasiewski, Simulation of passive microwave wind direction signatures over the ocean using an asymmetric-wave geometrical optics model, *Radio Sci.*, 32, 59–78, 1997.
- Lamarre, E., and W. K. Melville, Instrumentation for the measurement of void-fraction in breaking waves-laboratory and field results, *IEEE J. Ocean Eng.*, 17, 204–215, 1992.
- Liu, Y., and X.-H. Yan, The wind induced wave growth rate and the spectrum of the gravity-capillary waves, *J. Phys. Oceanogr.*, 25, 3196–3217, 1995.
- Longuet-Higgins, M. S., The statistical analysis of a random moving surface, *Proc. R. Soc. London, Ser. A*, 249, 321–387, 1957.
- Longuet-Higgins, M. S., On wave breaking and the equilibrium spectrum of wind generated waves, *Proc. R. Soc. London, Ser. A*, 310, 151–159, 1969.
- Longuet-Higgins, M. S., A stochastic model of sea-surface roughness: I. Wave crests, *Proc. R. Soc. London, Ser. A*, 410, 19–34, 1987.
- Longuet-Higgins, M. S., and J. S. Turner, An 'entraining plume' model of a spilling breaker, *J. Fluid Mech.*, 63, 1–20, 1974.
- Makin, V. K., and V. N. Kudryavtsev, Impact of dominant waves on sea drag, *Boundary Layer Meteorol.*, 103, 83–99, 2002.
- Melville, W. K., Energy dissipation by breaking waves, *J. Phys. Oceanogr.*, 24, 2041–2049, 1994.
- Melville, W. K., and P. Matusov, Distribution of breaking waves at the ocean surface, *Nature*, 417, 58–63, 2002.
- Meza, E., J. Zhang, and R. J. Seymour, Free-wave energy dissipation in experimental breaking waves, *J. Phys. Oceanogr.*, 30, 2404, 2000.
- Monahan, E., Oceanic whitecaps, *J. Phys. Oceanogr.*, 1, 139, 1971.
- Monahan, E. C., Whitecap coverage as a monitorable indication of the rate of bubble injection into the oceanic mixed layer, in *Sea Surface Sound*, Kluwer Acad., Norwell, Mass., 1988.
- Monahan, E., Oceanic whitecaps: Sea surface features detectable via satellite that are indicators of the air-sea gas transfer coefficient, *Earth Planet. Sci.*, 111, 315–319, 2002.
- Monahan, E., and I. G. O'Muircheartaigh, Optimal power-law description of oceanic whitecap coverage dependence on wind speed, *J. Phys. Oceanogr.*, 10, 2094–2099, 1980.
- Monahan, E., and D. K. Woolf, Comments on variations of whitecap coverage with wind stress and water temperature, *J. Phys. Oceanogr.*, 19, 706–709, 1989.
- Monahan, E., and C. R. Zietlow, Laboratory comparisons of fresh-water and salt-water whitecaps, *J. Geophys. Res.*, 74, 6961–6966, 1969.
- Norberg, W., J. Conaway, D. B. Ross, and T. Wilheit, Measurements of microwave emission from a foam-covered, wind-driven sea, *J. Atmos. Sci.*, 429–435, 1971.
- Ochi, M. K., and C.-H. Tsai, Prediction of occurrence of breaking waves in deep water, *J. Phys. Oceanogr.*, 13, 2008–2019, 1983.
- Pandey, P. C., and R. K. Kakar, An empirical microwave emissivity model for a foam-covered sea, *IEEE J. Oceanic Eng.*, OE-7, 135–140, 1982.
- Phillips, O., Spectral and statistical properties of the equilibrium range in the wind-generated gravity waves, *J. Fluid Mech.*, 156, 505–531, 1985.
- Phillips, O., F. L. Posner, and J. P. Hansen, High range resolution radar measurements of the speed distribution of breaking events in wind-generated ocean waves: Surface impulse and wave energy dissipation rates, *J. Phys. Oceanogr.*, 31, 450–460, 2001.
- Plant, W. J., A relationship between wind stress and wave slope, *J. Geophys. Res.*, 87, 1961–1967, 1982.
- Rapp, R. J., and W. K. Melville, Laboratory measurements of deep-water breaking waves, *Philos. Trans. R. Soc. London, Ser. A*, 331, 735–780, 1990.
- Rosenkranz, P. W., and D. H. Staelin, Microwave emissivity of ocean foam and its effect on nadir radiometric measurements, *J. Geophys. Res.*, 77, 6528–6537, 1972.
- Ross, D. B., and V. Cardone, Observations of oceanic whitecaps and their relation to remote measurements of surface wind speed, *J. Geophys. Res.*, 79, 444–452, 1974.
- Sharkov, Y. A., Experimental investigations of the lifetime for breaking wave dispersive zone, *Izv. Atmos. Oceanic Phys.*, 30, 808–811, 1995.
- Smith, P. M., The emissivity of sea foam at 19 and 37 GHz, *IEEE Trans. Geosci. Remote Sens.*, 26, 541–547, 1988.
- Srokosz, M., On the probability of wave breaking in deep water, *J. Phys. Oceanogr.*, 16, 382–385, 1986.
- Stogryn, A., The emissivity of sea foam at microwave frequencies, *J. Geophys. Res.*, 77, 1658–1666, 1972.
- Tang, C. C. H., The effect of droplets at the air-sea transition zone on the sea brightness temperature, *J. Phys. Oceanogr.*, 4, 579–593, 1974.
- Terrill, E., W. K. Melville, and D. Stramski, Bubble entrainment by breaking waves and their influence on optical scattering in the upper ocean, *J. Geophys. Res.*, 106, 16,815–16,823, 2001.
- Ulaby, F., R. Moore, and A. Fung, *Microwave Remote Sensing: Active and Passive*, vol. 3, Artech House, Norwood, Mass., 1986.
- Vagle, S., and D. M. Farmer, Measurement of bubble-size distributions by acoustical backscatter, *J. Atmos. Oceanic Technol.*, 9, 630–644, 1992.
- VanMelle, M. J., H. H. Wang, and W. F. Hall, Microwave radiometric observations of simulated sea surface conditions, *J. Geophys. Res.*, 78, 969–976, 1973.
- Walker, R. E., *Marine Light Field Statistics*, John Wiley, Hoboken, N.J., 1994.
- Wang, Q., E. C. Monahan, W. Asher, and P. M. Smith, Correlation of whitecap coverage and gas transfer velocity with microwave brightness temperature for plunging and spilling breaking waves, in *Air-Water Gas Transfer*, edited by B. Jähne and E. C. Monahan, pp. 869–878, AEON Verlag and Studio, Heidelberg Univ., Heidelberg, Germany, 1995.
- Webster, W. J., T. T. Wilheit, D. B. Ross, and P. Gloersen, Spectral characteristics of the microwave emission from a wind-driven foam covered sea, *J. Geophys. Res.*, 81, 3095–3099, 1976.
- Wilheit, T. T., A model for the microwave emissivity of the ocean's surface as a function of wind speed, *IEEE Trans. Geosci. Electron.*, GE-17, 244–249, 1979.
- Williams, G. F., Microwave emissivity measurements of bubbles and foam, *IEEE Trans. Geosci. Electron.*, October, 221–224, 1971.
- Wu, J., Variation of whitecap coverage with wind stress and water temperature, *J. Phys. Oceanogr.*, 18, 1448–1453, 1988.
- Xu, D., X. Liu, and D. Yu, Probability of wave breaking and whitecap coverage in a fetch-limited sea, *J. Geophys. Res.*, 105, 14,253–14,259, 2000.
- Zheng, Q. A., V. Klemus, and Y. H. L. Hsu, Laboratory measurements of water surface bubble life time, *J. Geophys. Res.*, 88, 701–706, 1983.
- Zhou, L., L. Tsang, and Q. Li, Effects of foam on the four Stokes parameters of passive microwave remote sensing of the ocean, paper presented at Progress in Electromagnetic Research Symposium, Mass. Inst. of Technol., Cambridge, Mass., 2002.

B. Chapron and N. Reul, Institut Français de Recherche pour l'Exploitation de la Mer, Laboratoire d'Océanographie Spatiale, BP 70, F-29280 Plouzané, France. (bchapron@ifremer.fr; nreul@ifremer.fr)